IEEE Access
Multidisciplinary | Rapid Review | Open Access Journal

Received August 10, 2020, accepted August 19, 2020, date of publication August 21, 2020, date of current version September 4, 2020.

Digital Object Identifier 10.1109/ACCESS.2020.3018620

Small-Signal Stability Analysis of Hybrid Power System With Quasi-Oppositional Sine Cosine Algorithm Optimized Fractional Order PID Controller

DIPAYAN GUHA[1], (Member, IEEE), PROVAS KUMAR ROY[2], (Member, IEEE), SUBRATA BANERJEE[3], (Senior Member, IEEE), SANJEEVIKUMAR PADMANABAN[4], (Senior Member, IEEE), FREDE BLAABJERG[5], (Fellow, IEEE), AND DHANAMJAYULU CHITTATHURU[4,6], (Member, IEEE)

[1]Electrical Engineering Department, Motilal Nehru National Institute of Technology Allahabad, Prayagraj 211004, India
[2]Electrical Engineering Department, Kalyani Government Engineering College, Kalyani 741235, India
[3]Electrical Engineering Department, National Institute of Technology Durgapur, Durgapur 713209, India
[4]Department of Energy Technology, Aalborg University, 6700 Esbjerg, Denmark
[5]Department of Energy Technology, Aalborg University, 9220 Aalborg, Denmark
[6]School of Electrical Engineering, Vellore Institute of Technology (VIT), Vellore 632014, India

Corresponding authors: Dipayan Guha (dipayan@mnnit.ac.in) and Sanjeevikumar Padmanaban (san@et.aau.dk)

This work was supported by the Danida Mobility Grant, responsible for the Ministry of Foreign Affairs of Denmark (MFA), Act 7 on Denmark's International Development Cooperation, under Project 19-MG06AAU.

ABSTRACT This article deals with the frequency instability problem of a hybrid energy power system (HEPS) coordinated with reheat thermal power plant. A stochastic optimization method called a sine-cosine algorithm (SCA) is, initially, applied for optimum tuning of fractional-order proportional-integral-derivative (FOPI-D) controller gains to balance the power generation and load profile. To accelerate the convergence mobility and escape the solutions from the local optimal level, quasi-oppositional based learning (Q-OBL) is integrated with SCA, which results in QOSCA. In this work, the PID-controller's derivative term is placed in the feedback path to avoid the set-point kick problem. A comparative assessment of the energy-storing devices is shown for analyzing the performances of the same in HEPS. The qualitative and quantitative evaluation of the results shows the best performance with the proposed QOSCA: FOPI-D controller compared to SCA-, grey wolf optimizer (GWO), and hyper-spherical search (HSS) optimized FOPI-D controller. It is also seen from the results that the proposed QOSCA: FOPI-D controller has satisfactory disturbance rejection ability and shows robust performance against parametric uncertainties and random load perturbation. The efficacy of the designed controller is confirmed by considering generation rate constraint, governor dead-band, and boiler dynamics effects.

INDEX TERMS Frequency stabilization, hybrid energy power system, Sine-Cosine algorithm, energy storage system, quasi-oppositional based learning, fractional order calculus.

NOMENCLATURE

AE	Aqua-electrolyzer
BESS	Battery energy storage system
DEPG	Diesel engine power generator
DG	Distributed generator
FC	Fuel cell
FESS	Flywheel energy storage system
FOPI-D	Fractional-order proportional integral-derivative
GDB	Governor dead-band
GRC	Generation rate constraint
HEPS	Hybrid energy power system
LFC	Load frequency control
MG	Microgrid
PV	Photovoltaic array
QOSCA	Quasi-oppositional sine cosine algorithm
RER	Renewable energy resource
RLP	Random load perturbation
SLD	Step load disturbance
T.F	Transfer function

The associate editor coordinating the review of this manuscript and approving it for publication was Mouloud Denai.

UC	Ultracapacitor
WTG	Wind turbine generator
n_p	Population size
dim	The dimension of the control variable
ub and lb	Upper and lower bounds, respectively, of search space
X_i^{k+1}	Position of i^{th} search agent at $(k+1)^{th}$ iteration
X_i^k	Position of i^{th} search agent at k^{th} iteration
rand	Uniformly generated a random number
T_i *and* T_d	Integral and derivative time constants, respectively
γ	The cut-off frequency of the low-pass filter
$C(s)$	Control output
$R(s)$	Reference input signal
$D(s)$	Disturbance input signal
$B(s)$	Feedback signal
$N(s)$	Noise signal
$U(s)$	Control signal
β	Integral fraction
ΔP_D	Load disturbance
$\Delta\Phi$	Variation of solar radiation
G_{WTG}	T.F. of wind turbine generator
G_{PV}	T.F. of photovoltaic array
G_{DEG}	T.F. of the diesel engine generator
G_{FC}	T.F. of fuel cell
G_{FESS}	T.F. of flywheel energy storage system
G_{BESS}	T.F. of battery energy storage system
G_{AE}	T.F. of aqua-electrolyzer
G_{UC}	T.F. of ultracapacitor
G_{ps}	T.F. of power system

I. INTRODUCTION

Modern power systems demand high intelligence and flexibility in control and optimization to guarantee its ability to match generation-load demand under load perturbation [1]. However, the gradual inanition of fossil fuels and the rise of fuel prices reveal that conventional power generations are incapable of matching the required load profile. One possible way of matching increasing load demand is by integrating renewable energy resources (RER) with a conventional power generator. The RERs like a photovoltaic array (PV), wind turbine generator (WTG), diesel engine generator (DEG), bio-fuels, etc. in the form of distributed generation (DG) is extensively used in today's power system. However, the PV-array has low energy conversion efficiency and costlier than WTG [2]. Fuel cell (FC) has gained attention in the recent past as an RER since it is environment-friendly, efficient, reusability of exhaust heat, etc. [3]. DEG is employed in the hybrid energy power system (HEPS) as a standby unit to adjust MW power with load demand during the impatience of wind and/or solar power. Owing to the intermittent characteristic of wind speed and solar radiation, a mismatch between power generation and demand is observed. The use of energy storing devices like a flywheel, battery storage, ultracapacitors (UC), etc. has gained impetus for improving the performance and stability degree of HEPS [4]. Pan and Das [6] utilized BESS, FESS, and UC in an autonomous HEPS. The efficacy of CES and RFB for damping of frequency and power oscillations of a three-area wind-hydro-thermal system is studied in [7]. The performance of SMES was considered in [8]. The comparative study of different energy storing devices is presented in [9]. However, this study only includes generation rate constraint (GRC) for studying the performance of energy storing devices. Thus, further research on the efficacy of energy-storing devices with more system nonlinearities (e.g., dead band, time-delay, etc.) is necessary.

In addition to load changes, the uncertain behavior of output power of WTG and PV farms causes deviation of system frequency from the nominal level. The control of area frequency with the governor-turbine mechanism is unsatisfactory due to its slow dynamics. If this undue deviation exists for a long time, there is a chance of damaging the auxiliary devices. Thus, to preserve system stability, various control methods were used in the literature [10]–[21]. A particle swarm optimization (PSO) based fuzzy-logic frequency controller was proposed in [10]. The whale optimization algorithm (WOA) tuned proportional-integral-derivative (PID) controller was developed in [13] to solve the frequency control problem of an interconnected modern power system. Guha *et al.* [16], in his recent endeavor, proposed multi-verse optimization (MVO) for load frequency control (LFC) of a four-area interconnected power system. The participation of electric vehicles in the load frequency control (LFC) scheme has been illustrated in [22]. The authors of [23] implemented a robust PI-controller for the LFC of power system with time-delay. Ameli *et al.* performed multi-stage frequency control of a microgrid (MG) with PSO optimized fuzzy aided PI-controller [24]. LFC of two-area interconnected power system equipped with PID-controller following wave energy disturbance is discussed in [25]. Three optimization techniques, namely teaching learning-based optimization (TLBO), harmony search (HS), and sine-cosine algorithm (SCA), were utilized for exploring the optimum gains of PID-controller [25]. Though implementation of the PID-controller is straightforward, however, its performance deteriorates with system nonlinearities and uncertainties.

Fractional order controller (FOC) has gained impetus due to its higher flexibility and effectiveness. The FOC deals with differential equations following fractional order calculus. The usefulness of FOC has been established for multi-area power system under deregulation [26], voltage control of distributed energy power system in islanded mode [27], flexible swing arm system [28], autonomous microgrid system [29], controlling voltage and rotor angle instability [30], etc. In [31], authors have developed FOPID-controller for voltage source inverter of an autonomous microgrid. The superiority of PSO optimized FOPID-controller is shown over integral order PID-controller in [32]. Mahto *et al.* implemented FOPID-controller for LFC of wind-biomass isolated HEPS [33]. An adaptive multi-objective fractional order fuzzy PID controller was designed for the LFC of islanded

MGs [34]. The effectiveness of an electric vehicle is also demonstrated in [34]. TLBO optimized FOPID-controller for LFC of an interconnected power system is studied in [35]. Salp swarm algorithm (SSA) optimized FOPID-controller was proposed in [36] for LFC of a two-area interconnected power system with a redox flow battery. The effectiveness of the FOPID-controller has also been shown in other control areas [37], [38]. Surprisingly none of these works was considered the set-point kick problem of conventional PID-controller while designing FOPID-controller. Thus, the application of FOPID-controller with the remedies of set-point kick and high-frequency amplification problems, in LFC, need to be reinvestigated. The performance of SCA in LFC of power systems is discussed in [9], [25], [40], [41]. The tuning compatibility of SCA for global optimization has been shown in [42]. An improved version of SCA with oppositional based learning has been tested for some benchmark functions and engineering problems in [43]. This work aims to introduce an advanced version of SCA called quasi-oppositional SCA (QOSCA). The objective of introducing quasi-oppositional based (Q-OBL) into SCA is to enhance the convergence mobility, computational accuracy, substantial improvement of the performance of SCA, avoiding optimal local levels, and minimizing computation time. The computational competence of QOSCA has been tested on HEPS linking with a reheat thermal power plant.

The notable contributions of the present work are summarized below.

- A linearized mathematical model (excluding nonlinearities and power energy converters) is developed to perform small-signal stability of HEPS. The developed HEPS is coordinated with reheat thermal power plant for frequency and power stability analysis.
- An optimized fractional-order proportional-integral-derivative (FOPI-D) controller is designed and included in the HEPS loop to resolve the frequency instability problem. The set-point kick and high-frequency amplification problems have been taken care of in the proposed FOPI-D controller.
- To derive excellent dynamic characteristics of HEPS, initially, SCA is applied for fine-tuning of FOPI-D controller gains. Afterward, to enhance the convergence rate and solution quality, Q-OBL has been hybridized with the original SCA resulting in QOSCA.
- A comparative study has been performed with original SCA, OSCA, hyper-spherical search (HSS), and grey wolf optimization (GWO) algorithms, recognized as powerful optimization methods in the literature, to show tuning competence of the proposed QOSCA,
- The system responses are analyzed with parameter uncertainties and random load perturbation (RLP) to affirm the robustness of the suggested controller.
- To show the FOPI-D controller's effectiveness, the consequences of GRC, governor dead-band, and boiler dynamics in the performance of HEPS have been studied.

The work presented in this article is organized as follows. Section 2 gives a mathematical model of different DGs following the model HEPS. The proposed SCA is discussed in Section 3. A brief theory of Q-OBL is also provided in Section 3. The simulation results and comparative analysis of the results are shown in Section 4. Finally, Section 5 gives concluding remarks with future extension and application of the present work.

II. MATHEMATICAL MODELLING OF HEPS

The hybrid power system comprising a PV array, DEG, FC with AE, and storage devices like FESS, BESS, and UC is considered for assessing the QOSCA optimized FOPI-D controller's performance. To perform a comparative analysis, the DGs are allowed to work in coordination with reheat thermal power plant. Fig 1(a) shows a single line diagram of MG with RERs. The RERs are connected to MG via the power conversion system. The linear approximated HEPS model for small-signal stability analysis is shown in Fig 1(b). The time constant of high-speed power electronic switches is neglected while modeling HEPS. However, to quantify the controller mastery, HEPS's dynamic stability has been assessed, incorporating inherent nonlinearities of the power system.

A. PHOTOVOLTAIC ARRAY (PV)

PV array consists of many cells connected in series and parallel to match the desired voltage and current. The output power of the PV array changes depending on solar radiation and/or load current. The output power of PV is calculated by using (1) [44].

$$P_{PV} = \eta A \Phi \left(1 - 0.005 \left(T_a + 25\right)\right) \tag{1}$$

where η is conversion efficiency ($9\% \leq \eta \leq 12\%$); A is an area of PV array; Φ is solar radiation in KW/m^2; T_a indicates the ambient temperature in °C. The transfer-function (T.F.) model of PV array for the small-signal stability analysis is defined as in (2) [4].

$$G_{PV}\left(s\right) = \frac{\Delta P_{PV}}{\Delta \Phi} = \frac{K_{PV}}{1 + sT_{PV}} \tag{2}$$

where ΔP_{PV} is the change of PV output power in pu; $\Delta\Phi$ is the change of solar radiation; K_{PV} and T_{PV} are the gain and time constant of PV array, respectively.

B. DIESEL ENGINE GENERATOR (DEG)

DEG is in action to provide the shortage of power in HEPS when PV array is incapable of matching the load demand. The T.F. model of DEG is shown in (3) [4], [5].

$$G_{DEG}\left(s\right) = \frac{\Delta P_{DEG}\left(s\right)}{u} = \frac{K_{DEG}}{1 + sT_{DEG}} \tag{3}$$

where ΔP_{DEG} is the incremental change of output power of DEG; K_{DEG} and T_{DEG} are the gain and time constant of DEG, respectively.

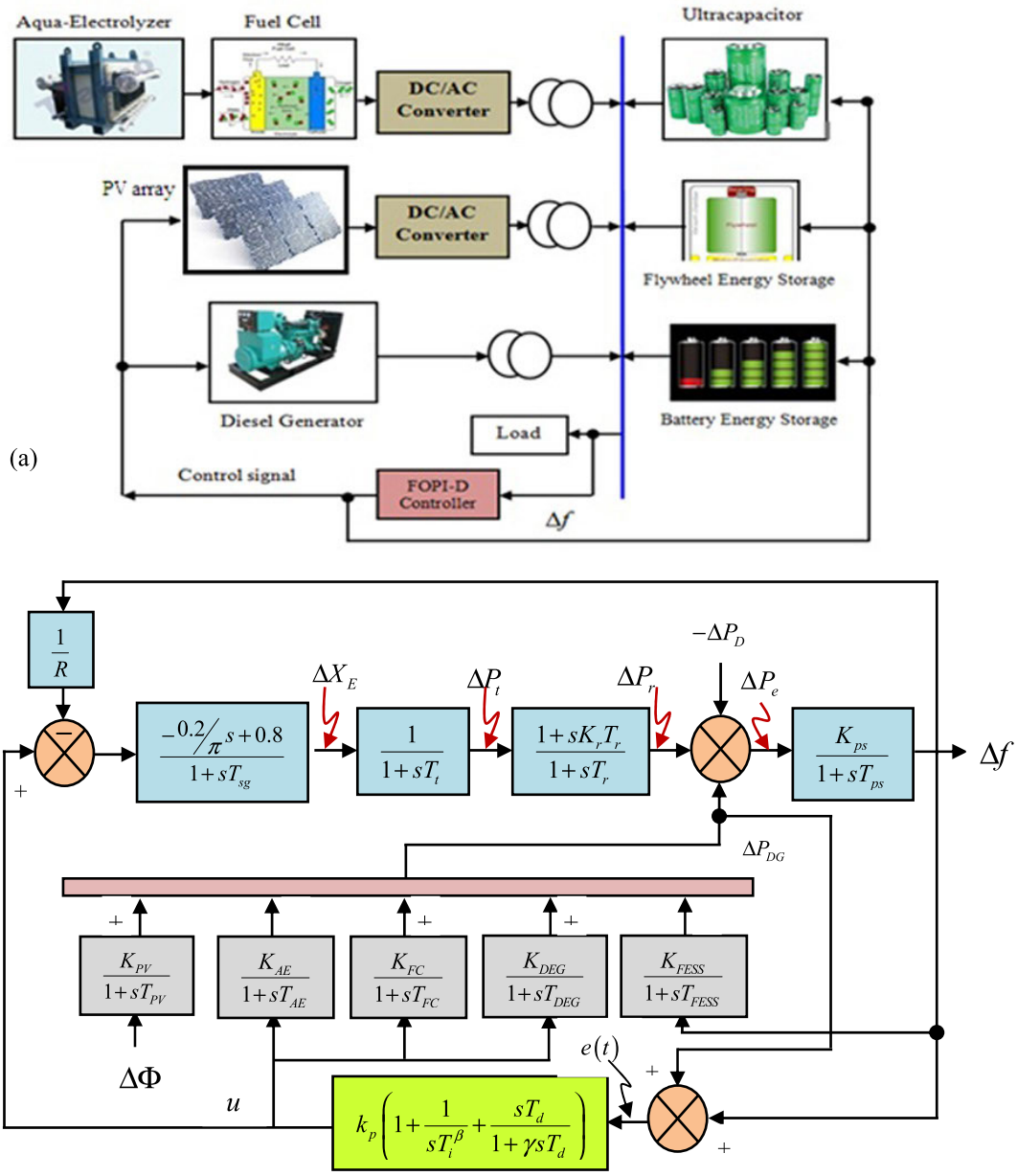

FIGURE 1. The hybrid energy power system (HEPS) model, (a) Single line diagram, (b) Block diagram of HEPS in coordination with reheat thermal power plant.

C. FUEL CELL (FC) AND AQUA-ELECTROLYZER (AE)

Fuel cells are an electrochemical device that produces DC electricity through hydrogen and oxygen reaction in the presence of an electrolyte. FC consists of (i) reformer (for producing hydrogen gas), (ii) a stack or a group of unit cells (the combination of electrolyte, separators, and plates), and (iii) a power conversion unit [3]. The T.F. model of FC is defined in (4).

$$G_{FC}(s) = \frac{\Delta P_{FC}(s)}{u_2} = \frac{K_{FC}}{1 + sT_{FC}} \tag{4}$$

where ΔP_{FC} is the incremental change of output power from FC; K_{FC} and T_{FC} are the gain and time constant of FC, respectively.

The AE absorbs rapidly fluctuating output power of PV and produces hydrogen in FC [4], [5] for the reaction. The T.F. model of AE for small-signal stability is given in (5).

$$G_{AE}(s) = \frac{\Delta P_{AE}(s)}{u_2} = \frac{K_{AE}}{1 + sT_{AE}} \tag{5}$$

where ΔP_{AE} is the incremental change of output power from AE; K_{AE} and T_{AE} are the gain and time constant of AE, respectively.

D. FLYWHEEL ENERGY STORAGE SYSTEM (FESS)

Flywheel energy storage system (FESS) stores electrical energy in the form of kinetic energy in the flywheel so that stored energy can release during the energy crisis. The merit

of FESS includes higher power density, insensitivity to the atmospheric conditions, free from hazardous chemicals, high conversion efficiency, high durability, etc. The energy stored in FESS is calculated by using (6) [4].

$$E_{FESS} = 0.5J\omega^2 \tag{6}$$

where J is the moment of inertia in $\left(Nm - s^2\right)$; ω indicates the rotational velocity of flywheel rotor in $rad/$ sec. The 1st order time-lag T.F. model of FESS is shown in (7) [4].

$$G_{FESS}(s) = \frac{\Delta P_{FESS}(s)}{u} = \frac{K_{FESS}}{1 + sT_{FESS}} \tag{7}$$

where ΔP_{FESS} is the incremental change of output power of FESS; K_{FESS} and T_{FESS} are the gain and time constant of FESS, respectively.

E. BATTERY ENERGY STORAGE SYSTEM (BESS)

Battery energy storage system (BESS) stores energy into a battery in the form of DC and releases it to the AC system through the power conversion system. However, it suffers from a low lifespan, minimum efficiency, and requires more auxiliary components for its operation. BESS is employed to add higher damping to the system oscillations for improving both transient and steady-state performances of the system. BESS consists of DC batteries connected to the AC system via transformer and power electronics converter. The T.F. description of BESS is shown in (8) [4].

$$G_{BESS}(s) = \frac{\Delta P_{BESS}(s)}{u} = \frac{K_{BESS}}{1 + sT_{BESS}} \tag{8}$$

where ΔP_{BESS} is the incremental change of output power from BESS; K_{BESS} and T_{BESS} are the gain and time constant of BESS, respectively.

F. ULTRACAPACITOR (UC)

An electric double-layer capacitor called supercapacitor (or electrochemical double layer capacitor or ultracapacitor) is an electrochemical capacitor that has high energy density as compared to conventional capacitors. The UC offers other options to smoothen the transient oscillations and matching the load profile. The merit of UC includes high efficiency, fast charging and discharge rate, high flexibility, and simple structure. The energy density of UC is much larger than the electrolyte capacitor, and their power density is almost ten times larger than the lead-acid battery [4], [5]. The stored charge in UC is calculated by using (9).

$$E_{UC} = 0.5\,C\left(V_{in}^2 - V_{final}^2\right) \tag{9}$$

where C is capacitance in Farad; V_{in} and V_{final} are initial and final voltages of UC. The T.F. model of UC considered for present study is shown in (10).

$$G_{UC}(s) = \frac{\Delta P_{UC}(s)}{u} = \frac{K_{UC}}{1 + sT_{UC}} \tag{10}$$

In (10), ΔP_{UC} is the incremental change of output power from UC; K_{UC} and T_{UC} are the gain and time constant of UC, respectively.

G. PROPORTIONAL-INTEGRAL-DERIVATIVE (PID) CONTROLLER

The proposed FOPI-D controller is a non-integer model of conventional PID-controller incorporated in the HEPS to improve the disturbance rejection ability of the system. The control law corresponding to PID-controller is given in (11).

$$U(s) = k_p\left[1 + \frac{1}{sT_i} + sT_d\right]E(s) \tag{11}$$

where k_p, T_i, and T_d are the proportional gain, integral, and derivative time constant, respectively; $e(t)$ is the error input to the controller.

Fig. 2(a) illustrates the block diagram of a closed-loop control system associated with conventional PID-controller. If the reference input to the controller has a step function, the manipulated signal will involve an impulse function, and thereby making the stability problem. This phenomenon is called a set-point kick. To avoid the set-point kick problem, the derivative block is placed in the feedback path, as shown in Fig. 2(b), so that the differentiation occurs only on the feedback signal. Again, the differentiating mode is highly sensitive to high-frequency noise. Thus, to attenuate high-frequency noise, an approximated derivative term, as shown in Fig. 2(b), is considered in the PID-control loop instead of pure derivative term. The term γ is the cut-off frequency of the low-pass filter, which is explored around 0.1 [45].

III. FRACTIONAL ORDER PROPORTIONAL-INTEGRAL-DERIVATIVE (FOPI-D) CONTROLLER

The concept of fractional order (FO) calculus was originated from the theory of generalizing the integral order (IO) calculus to FO calculus [46]. The most generally used FO integrodifferential definitions are based on Rieman-Liouville (RL), Grunwald-Letnikov, and Caputo expressions.

The RL fractional order integration and derivative, commonly used by the researchers, are defined in (12)-(13) [26], [31], in order.

$${}_bD_t^{\alpha} g(t) = \frac{1}{\Gamma(\alpha)}\int_b^t (t-\tau)^{\alpha-1}\, g(\lambda)\, d\lambda \tag{12}$$

$${}_bD_t^{\alpha} g(t) = \frac{1}{\Gamma(n-\alpha)}\frac{d^n}{dt^n}\int_b^t (t-\tau)^{n-\alpha-1}\, g(\lambda)\, d\lambda \tag{13}$$

where ${}_bD_t^{\alpha}$ is the fractional operator; $\Gamma(.)$ is Euler's gamma function; α $(\in (n-1, n))$ is proper fraction; n is an integer. To examine the dynamic behavior of the plant, T.F. model of the entire closed-loop control system needs to be developed employing Laplace transform. The general form of Laplace transforms for the integrodifferential equation is given in (14) [31].

$$L\left(\frac{d^n}{dt^n}g(t)\right) = s^n G(s) - \sum_{k=0}^{m-1} s^k\left[\frac{d^{m-1-k}}{dt^{n-1-k}}g(t)\right]_{t=0} \tag{14}$$

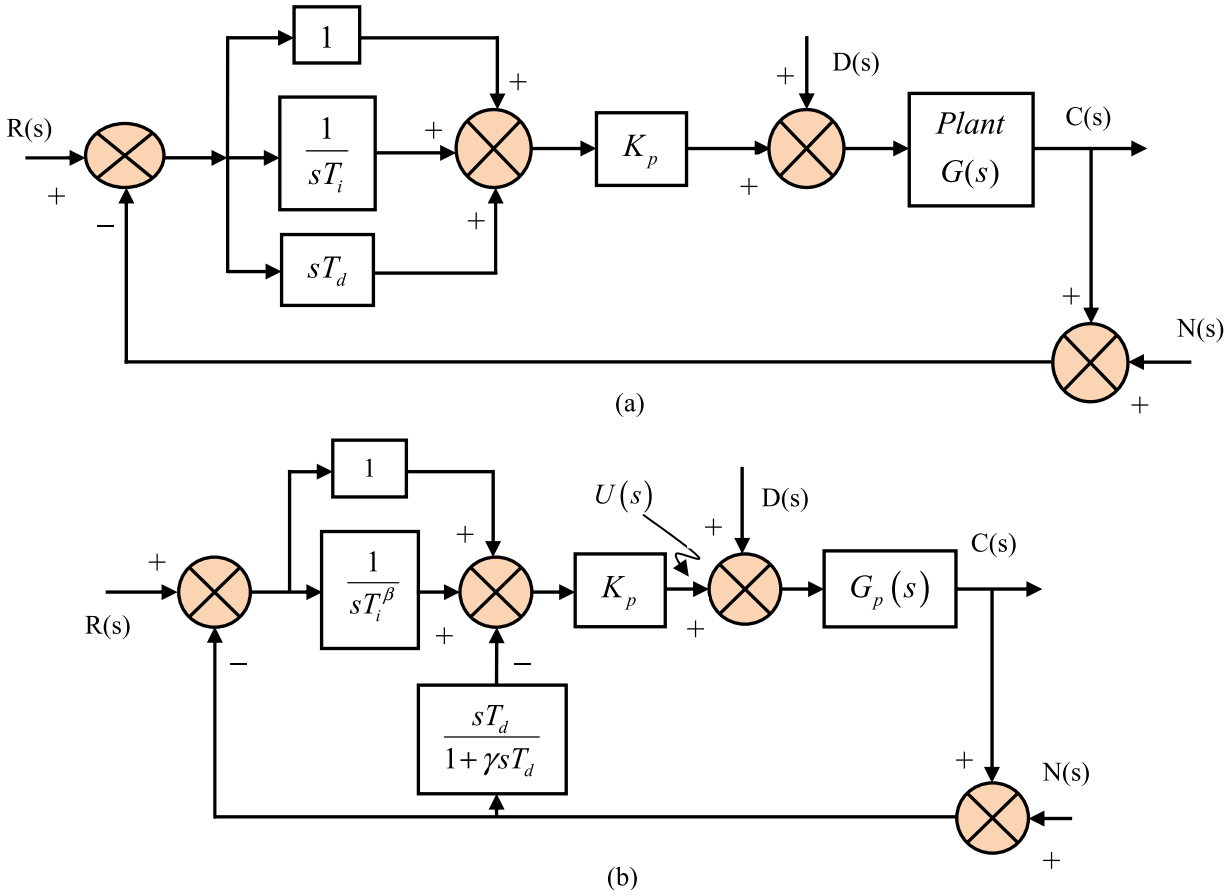

FIGURE 2. (a) Block diagram of conventional PID-controller, (b) Block diagram of PI-D controller with fractional integral action.

Assuming all the initial derivatives to zero, (14) is simplified as

$$L\left(\frac{d^n}{dt^n}g(t)\right) = s^n G(s) \tag{15}$$

Since the simulation and/or hardware implementation of a system with fractional order T.F. is not straightforward, hence some approximations have been taken to compute the integer-order T.F. Oustaloup filter approximation is the most common approximation taken by the researchers to represent a fractional-order T.F. into an integer order T.F. [34]. The general expression of the same within a frequency range $[\omega_l, \omega_h]$ is defined by (16) [26].

$$G(s) = s^{\alpha} = K\prod_{i=1}^{M}\frac{1+{}^{s}/_{\omega_{z,i}}}{1+{}^{s}/_{\omega_{p,i}}} \tag{16}$$

where K is adjustable system gain; M is the total number of poles and zeros; $\omega_{z,i}$ *and* $\omega_{p,i}$ are the frequencies of the i^{th} pole and zero. The small value of M leads to a simpler approximation, but introduces ripples in the responses. Conversely, the high value of M may eliminates the noise but makes a complex approximation.

In this work, authors have designed a fractional-order PID-controller (FOPI-D) considering the non-integer power of integrator for frequency stabilization of HEPS. The model of the proposed FOPI-D controller is shown in Fig. 2(b). The manipulated signal for the developed FOPI-D controller is generated, as shown in (17).

$$U(s) = K_p\left(1+\frac{1}{sT_i^{\beta}}\right)R(s) - K_p\left(1+\frac{1}{sT_i^{\beta}}+\frac{sT_d}{1+\gamma sT_d}\right)B(s) \tag{17}$$

The T.F. of closed-loop control system (Fig. 2(b)) following $D(s)$ as input is given in (18).

$$\left.\begin{aligned}\frac{C(s)}{D(s)} &= \frac{G_p(s)}{1+K_pG_p(s)\left(1+\frac{1}{sT_i^{\beta}}+\frac{sT_d}{1+\gamma sT_d}\right)}\\ \Rightarrow \frac{C(s)}{D(s)} &= \frac{G_p(s)}{1+G_p(s)G_c(s)} \quad R(s)=0; N(s)=0\end{aligned}\right\} \tag{18}$$

$$G_c(s) = K_p\left(1+\frac{1}{sT_i^{\beta}}+\frac{sT_d}{1+\gamma sT_d}\right) \tag{19}$$

where $G_p(s)$ is the plant T.F.; G_c is T.F. of FOPI-D controller; K_p indicates proportional gain; T_i is the integral time constant; β is integral fraction selected between (0, 1). The system is shown in Fig. 1(b) has two inputs, i.e., load

TABLE 1. Nominal values of DGs parameter with kW rating.

DG unit	kW rating	Parameter	Value	Parameter	Value	Parameter	Value
PV array	30	D	0.015 pu/Hz	T_{BESS}	1 sec	P_L	200
FC	70	$2H$	0.1667 pu sec	K_{PV}	1	R	2 Hz/MW
DEPG	160	T_g	0.08 sec	T_{PV}	1.8 sec	T_{DEG}	2 sec
FESS	45	T_t	0.4 sec	K_{FC}	0.01	f	50 Hz
BESS	45	K_{UC}	− 0.7	T_{FC}	4 sec	T_{FESS}	0.1 sec
UC	45	T_{UC}	0.9 sec	T_{AE}	0.5 sec	T_{AE}	0.5 sec
K_{FESS}	− 0.01	T_{AE}	0.5 sec	K_{BESS}	− 0.003	K_{DEG}	0.003

perturbation (ΔP_D) and solar radiation variation ($\Delta\Phi$). The closed-loop T.F. of HEPS following ΔP_D as input is defined in (20).

$$\frac{\Delta f}{\Delta P_D} = -\frac{G_{ps}}{1-\left(GG_c + \frac{(1+GG_c)G_{DG}G_c}{1-G_{DG}G_c} - \frac{G}{R}\right)G_{ps}} \tag{20}$$

In (20), $G_{ps}\left(=\frac{K_{ps}}{1+sT_{ps}}\right)$ is the T.F. of the power system; R represents speed regulation parameter of speed governor; G_{DG} and G are T.F. of DG unit and reheat thermal power plant, respectively, and calculated from (21).

$$\left.\begin{aligned} G_{DG} &= \frac{K_{DEG}K_{AE}K_{FC}}{(1+sT_{DEG})(1+sT_{AE})(1+sT_{FC})} \\ G &= \frac{(1+sK_rT_r)}{(1+sT_{sg})(1+sT_t)(1+sT_r)} \end{aligned}\right\} \tag{21}$$

where K_r & T_r are the gain and time constant of reheater, respectively; T_{sg} & T_t are time constants of speed governor and reheat turbine, respectively; K_{ps} & T_{ps} are gain and time constant of the power system, respectively. Similarly, the closed-loop T.F. of HEPS following $\Delta\Phi$ as input is calculated by using (22). Nominal values of system parameters, as depicted in Fig. 1(b) with the rated capacity of DGs are tabulated in Table 1 [1].

$$\frac{\Delta f}{\Delta\Phi} = \frac{\left(\frac{G_{PV}(1+G_cG)G_{ps}}{1-G_{DG}G_c}\right)}{1-\left(GG_c - \frac{G}{R}\right)G_{ps} - \left(\frac{G_{DG}G_c(1+G_cG)G_{ps}}{1-G_{DG}G_c}\right)} \tag{22}$$

IV. OPTIMIZATION TECHNIQUE

A. SINE-COSINE ALGORITHM (SCA)

The proposed SCA generates multiple random solutions and utilized them to fluctuate inward or outward of search boundaries employing two trigonometric functions, i.e., sine and cosine functions [39]. Like other EAs, SCA generates initial populations randomly by using (23).

$$\left.\begin{aligned} &for\ i = 1 : n_p \\ &\quad for\ j = 1 : \dim \\ &\qquad X(i,j) = lb + rand\,(ub - lb)\,; \\ &\quad end \\ &end \end{aligned}\right\} \tag{23}$$

In (23), n_p is population size; dim indicates the number of control variables; *rand* is uniformly generated random number; *ub* & *lb* are upper and lower bounds of control variables, respectively. The position of search agents is updated employing (24) [39].

$$\begin{cases} X_i^{k+1} = X_i^k + \left(a - \frac{k^*a}{iter_{\max}}\right) sin\,(r_1) \times \left|2^*rand - X_i^k\right|; \\ \qquad rand < 0.5 \\ X_i^{k+1} = X_i^k + \left(a - \frac{k^*a}{iter_{\max}}\right) \cos\,(r_1) \times \left|2^*rand - X_i^k\right|; \\ \qquad rand \geq 0.5 \end{cases} \tag{24}$$

where r_1 $(= 2\pi^*rand\,(0, 1))$ is a random number; a is a constant number; k and $iter_{\max}$ are current iteration, and maximum iteration counts, respectively.

B. QUASI-OPPOSITIONAL BASED LEARNING (Q-OBL)

This section discusses quasi-oppositional based learning (Q-OBL) integrated into original SCA for accelerating convergence rate and exploring better optimal gains of the FOPI-D controller. The initial population in SCA is generated randomly within the defined search area, and hence, update the positions of search agents by using (23).

Since the initialization process is entirely stochastic, thus, attaining the optimal global value is time-consuming. Furthermore, the solutions may quickly get trap at the local point. Therefore, to enhance the convergence mobility and escort the solutions from the local point, Q-OBL is housed with the original SCA. The effectiveness of the integration of Q-OBL in different EAs has already been verified in [47]–[49]. However, it has not been applied in SCA for the LFC of a power system. In OBL, initial guess and opposite numbers are simultaneously generated in a d-dimensional search space by using (25) [43].

$$\left.\begin{aligned} OX_j &= u_j + l_j - X_j; \\ OX_j \in [u, l]\,; &\quad j = 1, 2, \ldots, \dim \end{aligned}\right\} \tag{25}$$

where u and l are the extreme points of the search space.

The literature review unfolds that quasi-opposite number has a higher probability of being closer to the global solution than the opposite number without any prior information [50]. The quasi-opposite population is generated at the center of the search space and the corresponding opposite population, which results in a further decrease of computation time and speed up the convergence mobility. The quasi-opposite population can generate by using (26) [47]. The flowchart of SCA in the light of Q-OBL is shown in Fig. 3.

$$QOX_j = rand\left(\frac{u_j + l_j}{2}, OX_j\right); \quad j = 1, 2, \ldots, \dim \tag{26}$$

V. RESULTS AND DISCUSSION

To show the competence of the proposed FOPI-D controller, different cases are studied in this section. The stability of HEPS has been carefully investigated following a

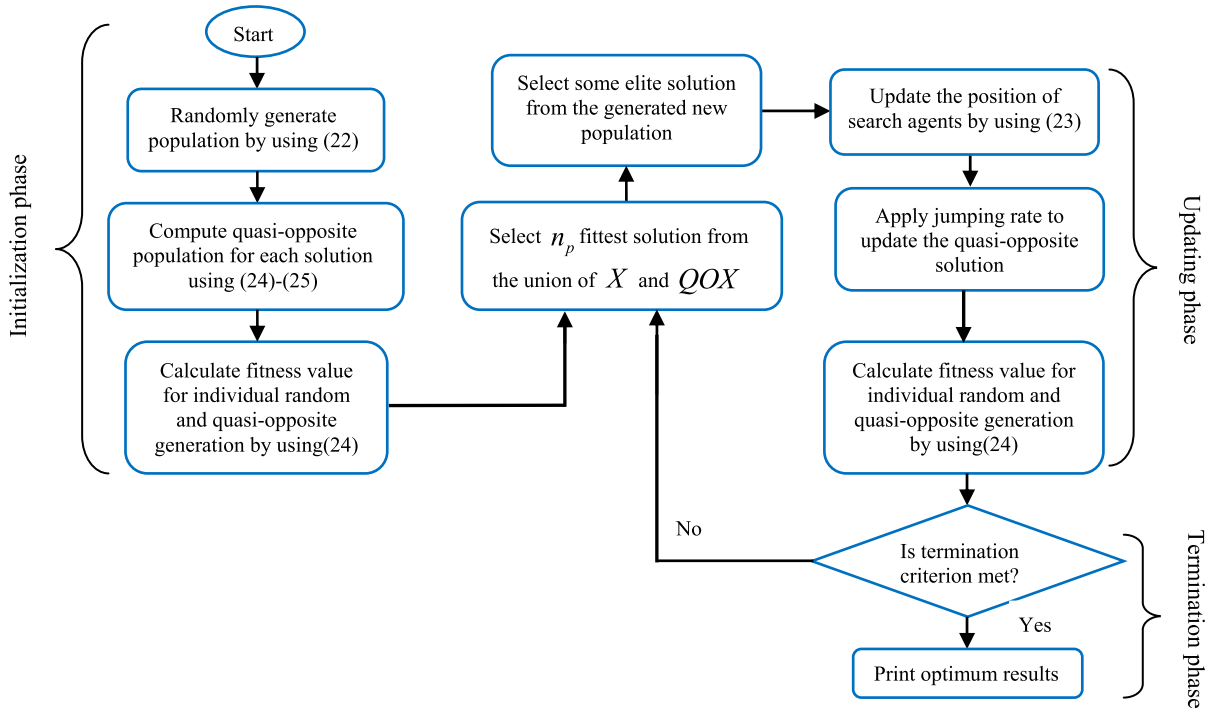

FIGURE 3. Flowchart of the proposed sine-cosine algorithm with Q-OBL.

TABLE 2. Controller settings and objective function values for different population size.

n_p	EAs	K_p	K_i	K_d	N	β	γ	J	ST	OS(x 10^{-4})
10	SCA	-1.9064	1.9818	-0.3924	92.0033	0.0477	0.0410	0.6669	7.49	4.39
	QOSCA	-1.8363	1.9978	-0.5422	10.0950	0.3981	0.0214	0.6558	7.41	5.61
20	SCA	-1.6787	1.9879	-0.5346	40.1179	0.3695	0.0799	0.6606	7.64	7.37
	QOSCA	-1.8342	1.8528	-0.2047	11.3478	0.3257	0.0159	0.6549	7.24	8.68
30	SCA	-1.8985	1.9732	-0.4210	177.3934	0.0282	0.0507	0.6669	7.65	4.51
	QOSCA	-1.7961	1.8859	-0.4523	5.3674	0.2974	0.0134	0.6542	6.97	9.32
40	SCA	-1.9013	1.9929	-0.3483	58.4352	0.0867	0.0994	0.6635	7.26	4.27
	QOSCA	**-1.9018**	**1.9919**	**-0.1248**	5.2806	**0.0367**	**5.2806**	**0.6440**	**6.48**	12
50	SCA	-1.9141	1.9185	-0.3712	86.7530	0.2686	0.0543	0.6677	7.60	4.29
	QOSCA	-1.9327	1.8463	-0.3543	6.3782	0.0734	0.0256	0.6443	6.53	11.24
60	SCA	-1.8736	1.9588	-0.4658	126.2182	0.7525	0.0248	0.6652	7.83	4.82
	QOSCA	-1.9156	1.9737	-0.3647	113.6873	0.4329	0.0236	0.6447	6.74	10.34

Boldface shows the best value

step increase of 1% in load and solar radiation variations. At the first instant, HEPS's performance integrated with FESS-BESS and FESS-UC is observed employing SCA optimized FOPI-D controller. To explore the effectiveness of energy storage devices, HEPS is also simulated without any energy storage devices. Afterward, to escape the solution from the local optimum level and accelerating convergence mobility of SCA, Q-OBL is hybridized with original SCA, which results in quasi-oppositional SCA (QOSCA). Since the primary objective of this study is to nullify the area frequency error, it is considered as an objective function for fine-tuning of controller gains. The literature review in this area reveals that an integral time absolute error (ITAE) based error criterion offers better results concerning time response specifications; hence it is used to define the fitness function for parameter optimization, which is given in (27). The simulations are performed on an Intel Core i3 2GB processor in the MATLAB R2013 environment. The SIMULINK model of HEPS is built-in SIMULINK environment, while the optimization code of SCA is written separately in *.m-file*.

$$J = \int_0^{iter_{\max}} |\Delta f|^* t^* dt \tag{27}$$

subjected to the constraints of: (i) controller parameters boundary, and (ii) proper selection of input parameters of SCA $(i.e.,\ n_p, iter_{\max})$, and (iii) jumping rate in Q-OBL.

Owing to the random nature of optimization techniques, 25 no's of trials were made before selecting the final FOPI-D controller gains. Table 2 presents a comparative study of

TABLE 3. Controller settings and time response specifications of HEPS with different energy storing devices.

Case studies		K_p	K_i	K_d	β	γ	N	J	RT	PT	OS (x10^{-4})	US	ST
$\Delta P_D = 0.01\,pu$	Without storage system	-1.9013	1.9929	-0.3483	0.0867	0.0994	58.4352	0.6635	**0**	0.3865	32	0.0149	7.33
	FESS-BESS	-1.8894	1.9544	-0.4492	0.3697	0.0103	130.1729	0.6563	**0**	0.3398	4.76	**0.0110**	7.78
	FESS-UC	-1.9570	1.9800	0.1449	0.4210	0.0554	5.1629	**0.6463**	**0**	**0.3699**	**4.27**	0.0118	**7.26**
$\Delta\Phi = 0.01\,pu$	Without storage system	0.8969	1.7080	0.2920	0.5807	0.0535	27.8938	0.0041	**0**	**1.06**	2.66	0.0049	13.85
	FESS-BESS	0.8913	1.7545	0.2565	0.1529	0.0759	25.1969	0.0039	**0**	1.13	2.57	**0.0046**	14.13
	FESS-UC	0.8610	1.9753	0.2502	0.6417	0.0439	14.5660	**0.0034**	**0**	1.13	**2.49**	0.0049	**13.79**

Boldface shows best value

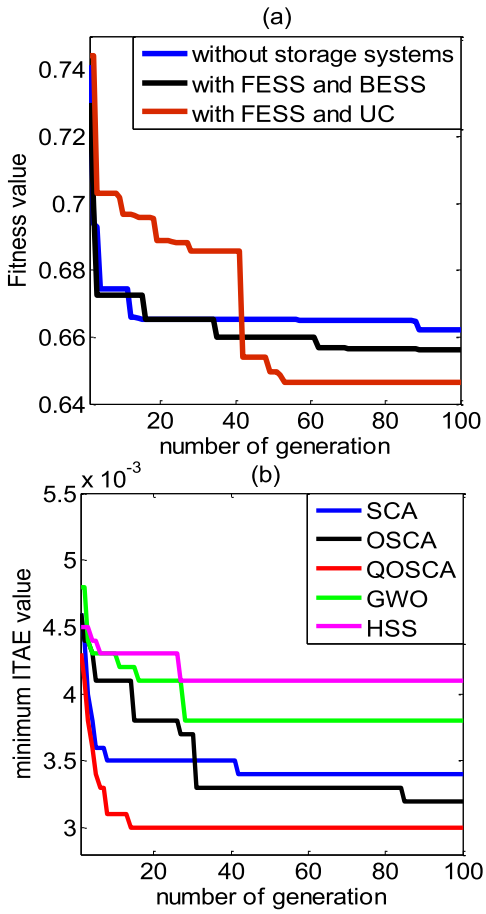

FIGURE 4. Convergence characteristics of (a) SCA with energy storage devices, (b) used evolutionary algorithms.

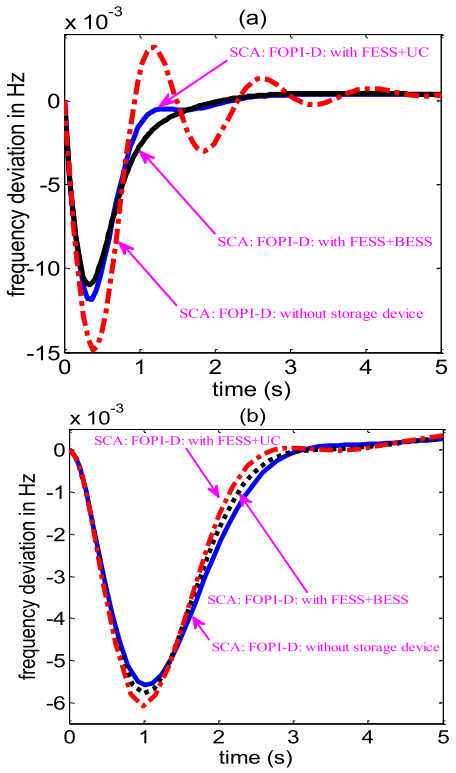

FIGURE 5. Performances of HEPS, (a) frequency variation with $\Delta P_D = 0.01\,pu$, (b) frequency variation with $\Delta\Phi = 0.01\,pu$.

different population sizes with SCA and QOSCA tuned FOPI-D controllers. Table 2 reveals that the least minimum fitness value, small settling time, and low peak overshoot of frequency response is obtained with $n_p = 40$. Moreover, a higher cost of population size degrades the convergence rate without improving the solution quality. Thus, $n_p = 40$ is chosen to perform the entire optimization. The convergence characteristic of the original SCA is shown in Fig. 4(a) considering different energy storing devices. It's viewed from Fig. 4(a) that SCA rapidly converges to the optimal global value and offers the least minimum value of error function when HEPS is coordinated with FOPI-D controller and FESS-UC storage devices compared to the value calculated with BESS-FESS and without storage devices. The results of Table 3 further confirm the above statement. The proposed SCA takes 60-70 iterations to converge into the optimal global value, which justifies the choice of maximum generation 100 for the present study.

Fig. 5 shows the frequency deviation of HEPS with the optimized controllers of Table 3 following load and solar radiation perturbations. The transient time measurements, such as rise time (RT), peak time (PT), overshoot (OS), undershoot (US), and settling time (ST), of Fig. 5 are shown in Table 3. It can be worth to note that time response specifications

TABLE 4. Comparative study of EAs for HEPS model coordinated with FESS-UC storage unit.

Case studies	Algorithms	K_p	K_i	K_d	β	γ	N	J	RT	PT	OS (x10^{-4})	US	ST
$\Delta P_D = 0.01\,pu$	SCA	-1.9570	1.9800	0.1449	0.4210	0.0554	5.1629	0.6463	**0**	0.3699	**4.27**	**0.0118**	7.26
	OSCA	-1.9570	1.9836	0.2386	0.4701	0.0747	9.6307	0.6458	**0**	0.3608	15	0.0146	7.43
	QOSCA	-1.9018	1.9919	-0.1248	0.4960	0.0367	5.2806	**0.6440**	**0**	**0.3424**	12	0.0152	**6.48**
	GWO	-1.8981	1.9652	-0.4244	0.1328	0.0228	122.7183	0.6525	**0**	0.3608	15	0.0146	7.43
	HSS	-1.9642	1.8904	-0.2148	0.6053	0.0565	187.7633	0.6761	**0**	0.3902	12	0.0139	7.90
$\Delta\Phi = 0.01\,pu$	SCA	0.8610	1.9753	0.2502	0.6417	0.0439	14.5660	0.0034	**0**	1.13	**2.49**	**0.0049**	13.79
	OSCA	0.8905	1.8083	0.2523	0.8103	0.0991	24.2819	0.0032	**0**	**1**	3.46	0.0060	13.03
	OOSCA	0.7898	1.9934	0.2546	0.7187	0.0469	16.6410	**0.0030**	**0**	**1**	3.57	0.0061	**12.32**
	GWO	0.9876	1.8200	0.2618	0.7874	0.0555	19.0700	0.0038	**0**	**1**	3.35	0.0056	13.34
	HSS	0.8969	1.7098	0.2585	0.6027	0.0515	18.7317	0.0041	**0**	1.1	3.57	0.0056	13.69

Boldface shows the best value

of HEPS using SCA: FOPI-D controller is lower when the system is coordinated with FESS-UC storage devices. Thus, it may conclude that the coordinated FESS-US provides faster damping to the frequency oscillations than coordinated FESS-BESS; and the rest of the study for HEPS is carried out with the coordinated FESS-US. Comparison of numerical results of Table 3 confirmed the supremacy of coordinated FESS-UC over FESS-BESS.

Fig. 4(b) depicts the convergence mobility of SCA, which is compared with the convergence characteristic of OSCA, QOSCA, GWO, and HSS algorithms. The minimum error function value calculated with SCA, OSCA, QOSCA, GWO, and HSS are provided and compared in Table 4. The optimal gains of the FOPI-D controller obtained with SCA, OSCA, QOSCA, GWO, and HSS are presented in Table 4. It is worthy to note from Table 4 that the convergence speed of SCA effectively increases with Q-OBL, which results in further minimization of the error function value. The dynamic response of HEPS obtained with SCA: FOPI-D controller is compared in Fig. 6 with the results obtained by OSCA, QOSCA, GWO, and HSS optimized FOPI-D controller. It can be noted that the system responses, using QOSCA: FOPI-D controller, are faster and have better damping characteristics than that obtained by SCA: FOPI-D, OSCA: FOPI-D, GWO: FOPI-D, and HSS: FOPI-D controllers. The results of Table 4 and Fig. 6 support the efficacy of QOSCA over original SCA, OSCA, GWO, and HSS to find the optimal settings of the FOPI-D controller for the proposed HEPS model.

The change of output power of different DGs with SCA: FOPI-D controller is shown in Figs. 7-8. To demonstrate the efficacy of proposed QOSCA: FOPI-D controller, the DGs output obtained with QOSCA: FOPI-D controller is also plotted in Figs. 7-8. It is seen from Fig. 7-8 that the proposed controllers, both SCA- and QOSCA-optimized FOPI-D controllers, are capable of restoring DGs output power to the steady-state value after the perturbations, and hence maintaining system stability. It is remarkable from Figs. 7-8 that the DGs output power obtained with SCA: FOPI-D controller exhibits more oscillations with high peak overshoot and undershoot. On the other hand, the responses quickly attained the steady-state level when QOSCA: FOPI-D controller is used in the HEPS loop. Thus, it may conclude that QOSCA: FOPI-D controller outperforms SCA: FOPI-D controller.

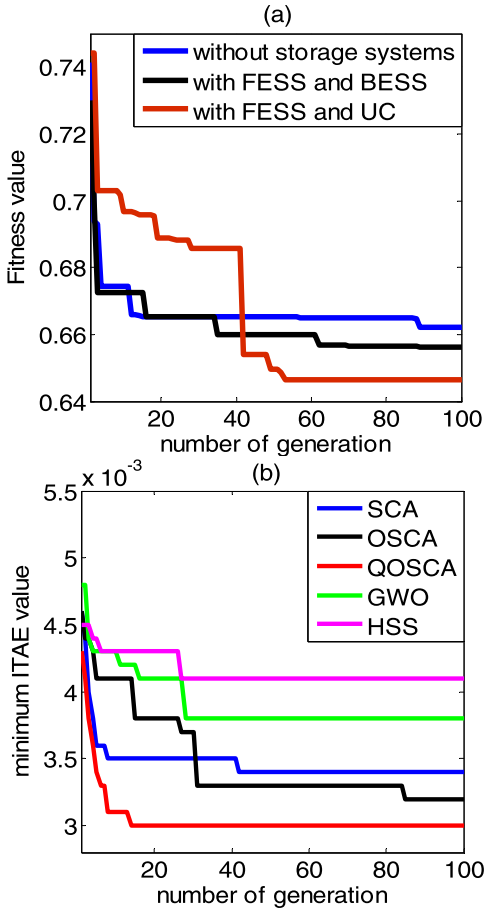

FIGURE 6. Comparative study of proposed EAs(a) frequency variation of HEPS with $\Delta P_D = 0.01\,pu$, (b) frequency variation of HEPS with $\Delta\Phi = 0.01\,pu$.

VI. ROBUSTNESS STUDY

Power system parameters are continually changing from their nominal settings, disturbing the nominal performance of HEPS. For affirming the robustness of the designed QOSCA: FOPI-D controller, system parameter of Fig. 1(b) is varied,

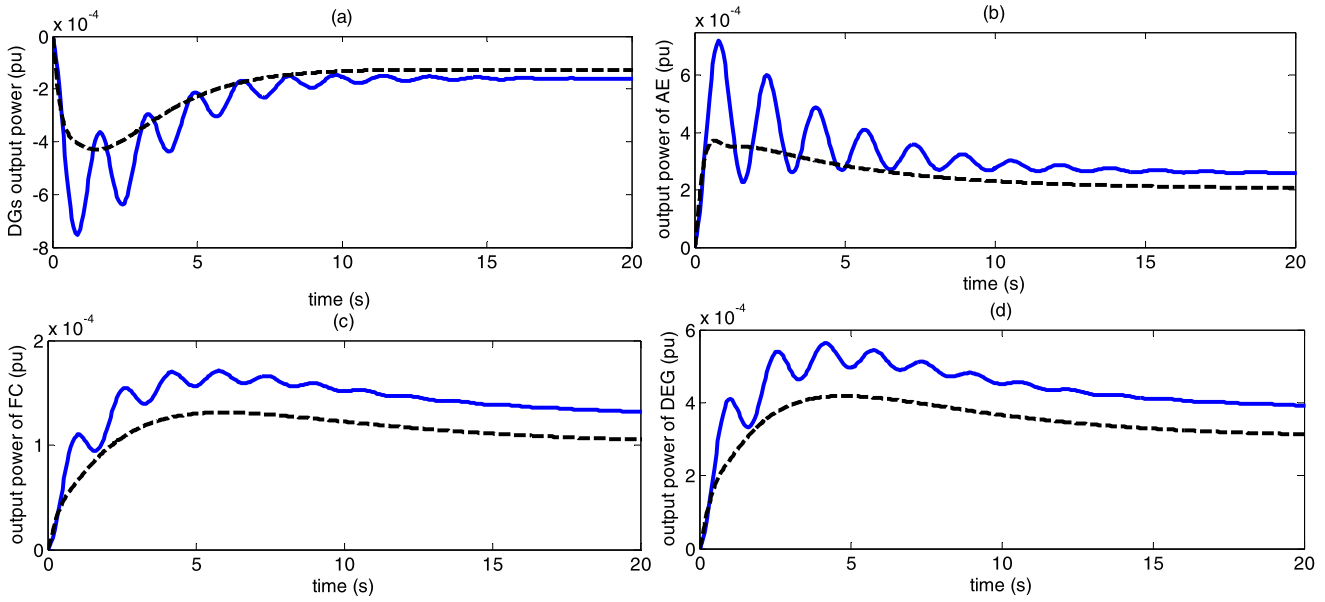

FIGURE 7. Output power of different DGs obtained with coordinated FESS-UC and FOPI-D controller following $\Delta P_D = 0.01\,pu$.

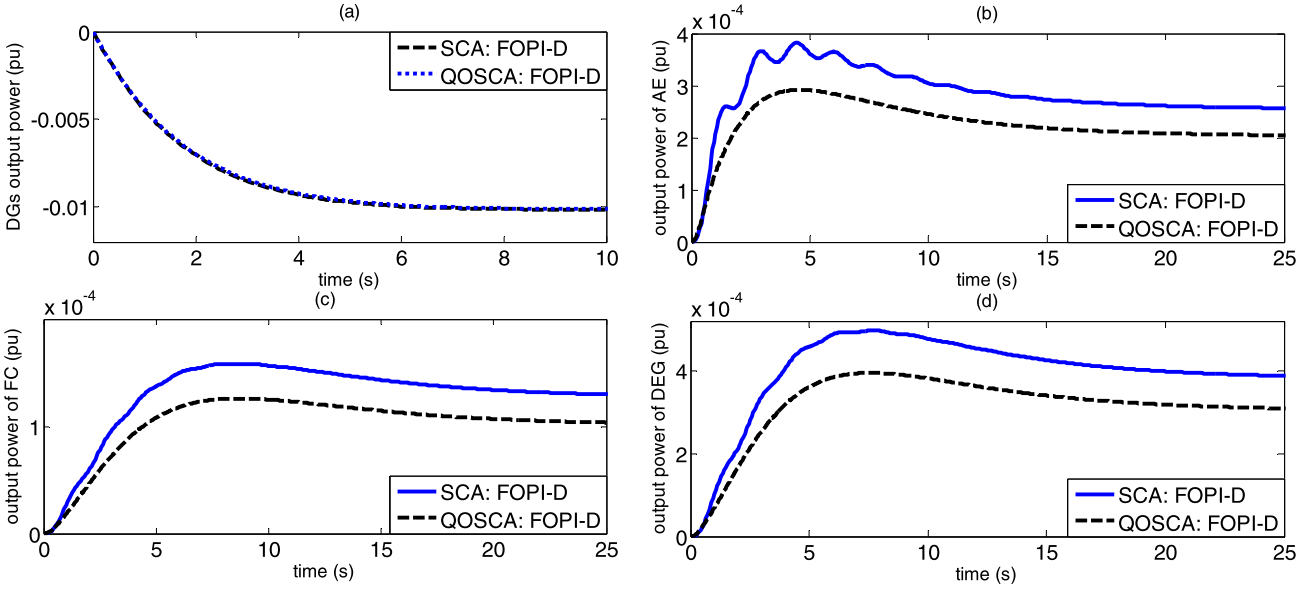

FIGURE 8. Output power of different DGs obtained with coordinated FESS-UC and FOPI-D controller following $\Delta\Phi = 0.01\,pu$.

according to Table 5. Since the superiority of QOSCA: FOPI-D controller has already been established in previous sections, the robustness of QOSCA: FOPI-D controller (Table 4) is investigated. This study further analyzes the sensitivity of the designed controller considering parameters variation. The deviation of frequency and power at normal and varied conditions is shown in Fig. 9 (a) and (b), respectively. It can worthy to note that the area frequency and power oscillations settle to the steady-state value nearly at the same time while the system parameter is changed according to Table 5. Only the change in the rise time is observed. Moreover, the change in peak overshoot is minimal with these variations. Thus, the robustness of the QOSCA: FOPI-D controller is confirmed. It can also conclude that the controller gains obtained at nominal condition need not be reset. A random load perturbation (RLP) with different magnitude and time instant, as shown in Fig. 10 (marked by blue color) is applied to HEPS for further analysis of the robustness of QOSCA: FOPI-D controller. The frequency deviation of HEPS following RLP is shown in Fig. 10. For better comparison, the results obtained with SCA: FOPI-D controller is also depicted in Fig. 10. It is noteworthy from Fig. 10 that

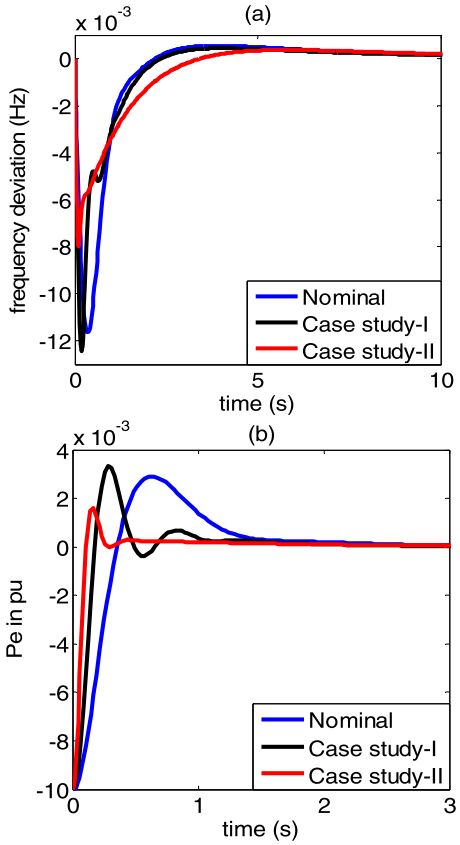

FIGURE 9. Dynamic performance of HEPS with QOSCA: FOPI-D controller considfering variation in system parameters, (a) frequency deviation, (b) ΔP_e deviation.

the proposed QOSCA: FOPI-D controller provides better damping to the system oscillations and quickly restores the disperse states to the steady-state value, as compared to SCA: FOPI-D controller.

TABLE 5. Uncertain parameters and variation range.

Case study-I			
Parameters	Variation	Parameters	Variation
R	+ 30%	T_{BESS}	+ 55%
T_{ps}	– 50%	T_t	– 50%
T_g	+ 50%	T_{FESS}	– 45%
Case study-II			
R	– 60%	T_{UC}	– 50%
T_{ps}	– 55%	T_t	– 53%
T_g	– 62%	T_{FESS}	– 35%

VII. STATISTICAL ANALYSIS

For statistical analysis, the optimization codes were run for 25 independent trials over the HEPS model with FESS-UC. The best, worst, mean, and standard deviations of the defined objective function are calculated with QOSCA and presented in Table 6. For comparison, the results of SCA, OSCA, GWO, and HSS algorithms are also provided in Table 6. Minute observation of the effects confirms the robustness and superiority of QOSCA over others.

VIII. PERFORMANCE STUDY WITH SYSTEM NONLINEARITIES

To establish the effectiveness of proposed QOSCA: FOPI-D controller, the performance of HEPS has been studied with power system nonlinearities, such as GRC, governor dead-band (GDB), and boiler dynamics (BD). A typical value of GRC of 3%/min for reheat thermal power plant is considered for analysis [51]. Backlash type of nonlinearity with a limiting amount of 0.06% is taken to describe the effects of GDB on system performance. The model of BD described

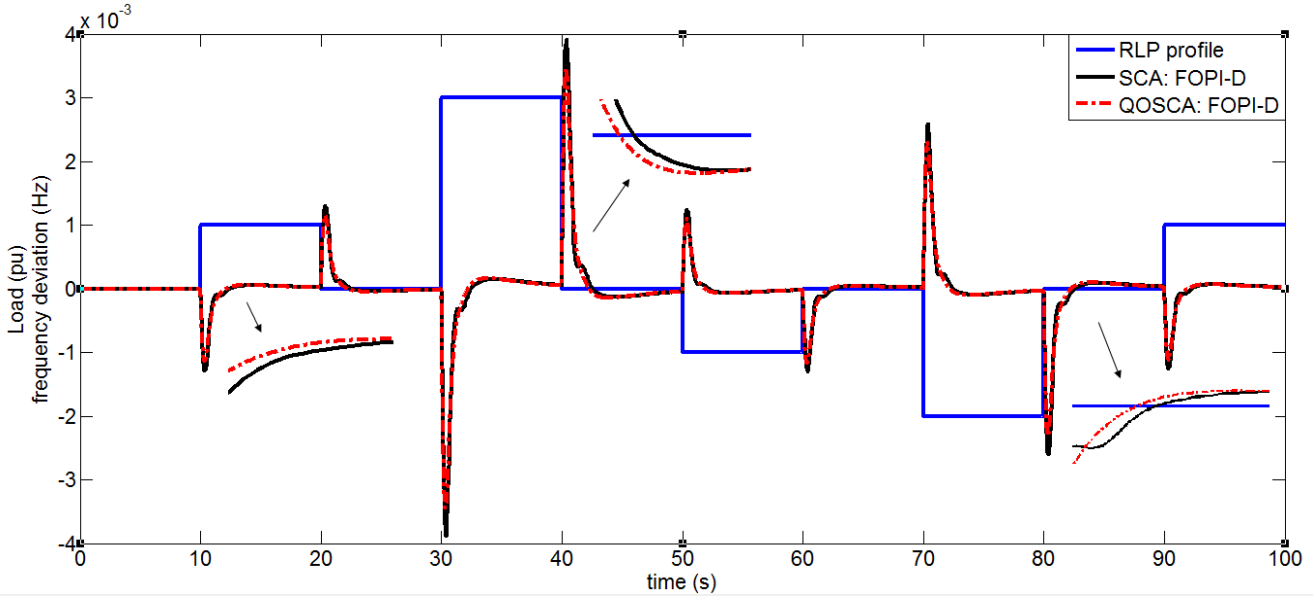

FIGURE 10. Frequency deviation of HEPS following RLP.

TABLE 6. Statistical results of proposed EAs.

Parameters	$\Delta P_D = 0.01\,pu$					$\Delta\Phi = 0.01\,pu$				
	SCA	OSCA	QOSCA	GWO	HSS	SCA	OSCA	QOSCA	GWO	HSS
Best	0.6463	0.6458	0.6440	0.6525	0.6761	0.0034	0.0032	0.0030	0.0038	0.0041
Worst	0.6525	0.6529	0.6508	0.6677	0.6867	0.0048	0.0046	0.0041	0.0051	0.0059
Mean	0.6503	0.6494	**0.6472**	0.6600	0.6804	0.0040	0.0038	**0.0035**	0.0045	0.0051
Standard deviation	0.0020	0.0021	**0.0018**	0.0048	0.0029	$4.5615\text{x}10^{-4}$	$3.6403\text{x}10^{-4}$	$\mathbf{2.901\text{x}10^{-4}}$	$3.706\text{x}10^{-4}$	$5.2337\text{x}10^{-4}$

TABLE 7. Transient specification of HEPS with system nonlinearities.

Case studies	Algorithms	RT	PT	OS	US	ST
With GDB	SCA	**0**	0.5637	0.0068	0.0297	14.58
	QOSCA	**0**	**0.5127**	**0.0012**	**0.0257**	**12.56**
With GDB + GRC	SCA	**0**	0.6018	0.0116	0.0312	31.29
	QOSCA	**0**	**0.5086**	**0.0010**	**0.0260**	**15.48**
With GDB + GRC + BD	SCA	**0**	0.7259	0.0115	0.0329	33.85
	QOSCA	**0**	**0.6205**	**0.0059**	**0.0320**	**18.78**

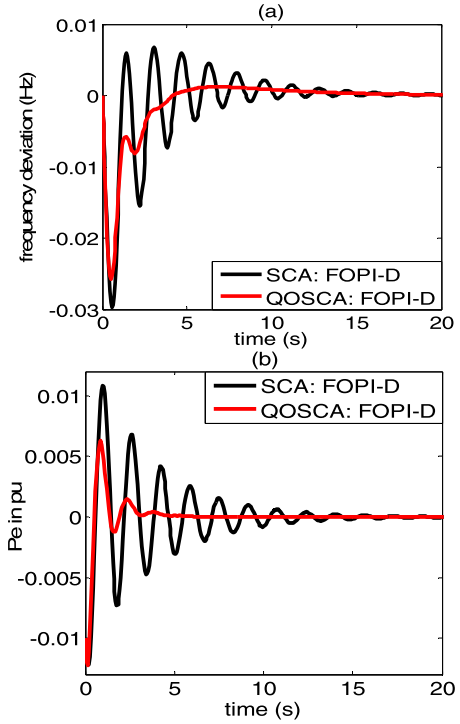

FIGURE 11. Dynamic performance of HEPS with GDB (a) frequency deviation, (b) ΔP_e variation.

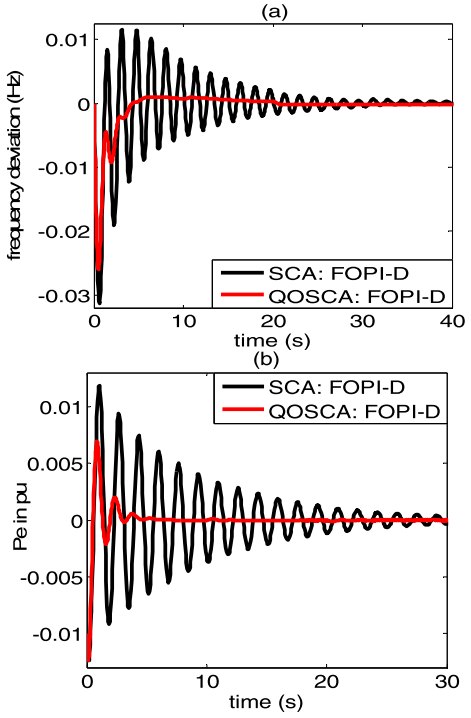

FIGURE 12. Dynamic performance of HEPS with GDB+GRC (a) frequency deviation, (b) ΔP_e variation.

in [52] is considered to study its impact. The optimized values of QOSCA: FOPI-D controller gains from Table 4 are considered to carry out the simulation. Figs. 11-13 shows the dynamic performances of HEPS, considering the nonlinearities mentioned above. The time response specifications of Figs. 11-13 are provided in Table 7. It is seen from the results that system oscillations, peak overshoot, and settling time of frequency and power responses are increased with nonlinearities. However, the designed QOSCA: FOPI-D controller is compatible with handling these nonlinearities and provides better results than obtained with the SCA: FOPI-D controller.

IX. CONCLUSION

An attempt has been made to study the frequency instability problem of a HEPS linked with reheat thermal power system and some energy storing devices. An optimized FOPI-D controller is applied to stabilize the frequency and output power deviation of HEPS following load and solar radiation perturbations. The set-point kick and high-frequency noise amplification problems were taken care of while developing the controller. The optimal gains of the FOPI-D controller are initially explored, employing the sine cosine algorithm (SCA). Furthermore, the Q-OBL mechanism has been integrated

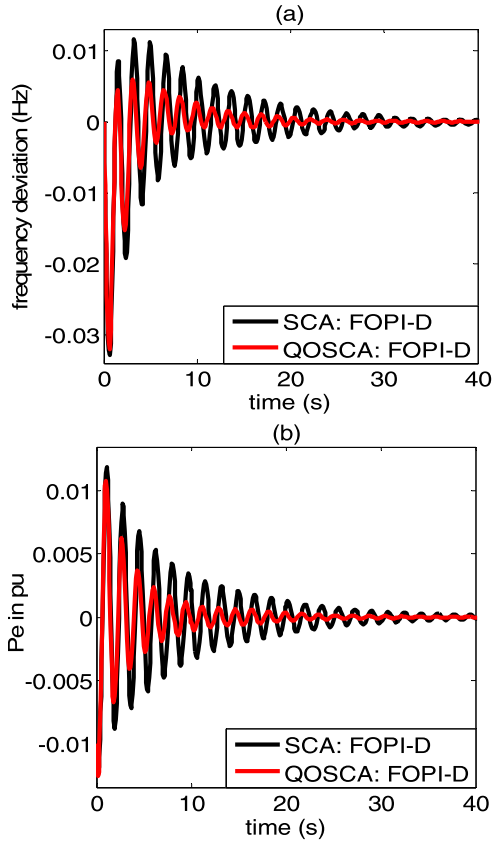

FIGURE 13. Dynamic performance of HEPS with GDB+GRC+BD (a) frequency deviation, (b) ΔP_e variation.

into SCA yields QOSCA for minimizing the computational complexities. Performance comparisons of QOSCA, OSCA, SCA, GWO, and HSS reflect better results concerning convergence rate, the minimum objective function value, settling time, peak overshoot, number of oscillations, and damping ratio are obtained using QOSCA: FOPI-D controller.

Moreover, the performance of coordinated FESS-UC for fast active compensation of system oscillations has been validated over FESS-BESS. The robustness of the proposed algorithm has been established by statistical analysis, sensitivity analysis, and RLP. The supremacy and effectiveness of QOSCA: FOPI-D controller has been confirmed with power system nonlinearities.

The study shows the effect of GRC, GDB, and BD nonlinearities on the system dynamics. However, detailed modeling, including more nonlinearities in the system, may give a better insight of controller performance. The computation time for finding optimal gains of the suggested controller is relatively more, and a high control effort is required to design the proposed controller. In the future, to minimize the controller design effort and simultaneously computation time, a suitable lower-order model of the test system (keeping the dominant features of the actual test system) shall be developed using appropriate model-order reduction techniques (e.g., balanced truncation algorithm). The proposed control strategy may be applied to a higher-order distributed power system for better assessment.

The future extension of the presented work is summarized as follows:

- The dynamic performance of HEPS may be examined considering other system nonlinearities (e.g., time-delay) and switching effects of power converters.
- The performance of different FACTS controllers in damping out HEPS oscillations may be a future extension of the present work.
- Although the proposed FOPI-D controller exhibits better performance, further improvement of the results may be made incorporating a disturbance observer to estimate the stochastic load variation and intermittent solar insolation (daily average) with it.
- Coordinated control strategy shall be developed with the deterministic/stochastic state observer for better outputs.
- The closed-loop robust stability of the studied test system may be examined by using Kharitonov's stability method.

REFERENCES

[1] H. Bevrani, F. Habibi, P. Babahajyani, M. Watanabe, and Y. Mitani, "Intelligent frequency control in an AC microgrid: Online PSO-based fuzzy tuning approach," *IEEE Trans. Smart Grid*, vol. 3, no. 4, pp. 1935–1944, Dec. 2012.

[2] T. Senjyu, T. Nakaji, K. Uezato, and T. Funabashi, "A hybrid power system using alternative energy facilities in isolated island," *IEEE Trans. Energy Convers.*, vol. 20, no. 2, pp. 406–414, Jun. 2005.

[3] Y. H. Kim and S. S. Kim, "An electrical modeling and fuzzy logic control of a fuel cell generation system," *IEEE Trans. Energy Convers.*, vol. 14, no. 2, pp. 239–244, Jun. 1999.

[4] P. K. Ray, S. R. Mohanty, and N. Kishor, "Proportional–integral controller based small-signal analysis of hybrid distributed generation systems," *Energy Convers. Manage.*, vol. 52, no. 4, pp. 1943–1954, Apr. 2011.

[5] V. P. Singh, S. R. Mohanty, N. Kishor, and P. K. Ray, "Robust H-infinity load frequency control in hybrid distributed generation system," *Int. J. Electr. Power Energy Syst.*, vol. 46, pp. 294–305, Mar. 2013.

[6] I. Pan and S. Das, "Fractional order fuzzy control of hybrid power system with renewable generation using chaotic PSO," *ISA Trans.*, vol. 62, pp. 19–29, May 2016.

[7] D. Saha and L. C. Saikia, "Performance of FACTS and energy storage devices in a multi area wind-hydro-thermal system employed with SFS optimized I-PDF controller," *J. Renew. Sustain. Energy*, vol. 9, no. 2, Mar. 2017, Art. no. 024103.

[8] S. Padhan, R. K. Sahu, and S. Panda, "Automatic generation control with thyristor controlled series compensator including superconducting magnetic energy storage units," *Ain Shams Eng. J.*, vol. 5, no. 3, pp. 759–774, Sep. 2014.

[9] W. Tasnin and L. C. Saikia, "Performance comparison of several energy storage devices in deregulated AGC of a multi-area system incorporating geothermal power plant," *IET Renew. Power Gener.*, vol. 12, no. 7, pp. 761–772, May 2018.

[10] N. Sa-ngawong and I. Ngamroo, "Intelligent photovoltaic farms for robust frequency stabilization in multi-area interconnected power system based on PSO-based optimal sugeno fuzzy logic control," *Renew. Energy*, vol. 74, pp. 555–567, Feb. 2015.

[11] M. Datta, T. Senjyu, A. Yona, T. Funabashi, and C.-H. Kim, "A frequency-control approach by photovoltaic generator in a PV–diesel hybrid power system," *IEEE Trans. Energy Convers.*, vol. 26, no. 2, pp. 559–571, Jun. 2011.

[12] M. Martínez, M. G. Molina, and P. E. Mercado, "Optimal sizing method of vanadium redox flow battery to provide load frequency control in power systems with intermittent renewable generation," *IET Renew. Power Gener.*, vol. 11, no. 14, pp. 1804–1811, Dec. 2017.

[13] H. M. Hasanien, "Whale optimisation algorithm for automatic generation control of interconnected modern power systems including renewable energy sources," *IET Gener., Transmiss. Distrib.*, vol. 12, no. 3, pp. 607–614, 2018.

[14] M. N. Ambia, H. M. Hasanien, A. Al-Durra, and S. M. Muyeen, "Harmony search algorithm-based controller parameters optimization for a distributed-generation system," *IEEE Trans. Power Del.*, vol. 30, no. 1, pp. 246–255, Feb. 2015.
[15] A. Teninge, C. Jecu, D. Roye, S. Bacha, J. Duval, and R. Belhomme, "Contribution to frequency control through wind turbine inertial energy storage," *IET Renew. Power Gen.*, vol. 3, no. 3, pp. 358–370, 2009.
[16] D. Guha, P. K. Roy, and S. Banerjee, "Multi-verse optimisation: A novel method for solution of load frequency control problem in power system," *IET Gener., Transmiss. Distrib.*, vol. 11, no. 14, pp. 3601–3611, Sep. 2017.
[17] N. Nikmehr and S. Najafi-Ravadanegh, "Optimal operation of distributed generations in micro-grids under uncertainties in load and renewable power generation using heuristic algorithm," *IET Renew. Power Gener.*, vol. 9, no. 8, pp. 982–990, Nov. 2015.
[18] B. Singh and S. Sharma, "Voltage and frequency controllers for standalone wind energy conversion systems," *IET Renew. Power Gener.*, vol. 8, no. 6, pp. 707–721, Aug. 2014.
[19] K. Nosrati, H. R. Mansouri, and H. Saboori, "Fractional-order PID controller design of frequency deviation in a hybrid renewable energy generation and storage system," in *Proc. 24th Int Conf Exhib. Elect. Distrib.*, vol. 2017, no. 1, pp. 1148–1152, 2017.
[20] T. S. Bhatti, A. A. F. Al-Ademi, and N. K. Bansal, "Load-frequency control of isolated wind-diesel-microhydro hybrid power systems (WDMHPS)," *Energy*, vol. 22, no. 5, pp. 461–470, May 1997.
[21] M. H. Andishgar, E. Gholipour, and R.-A. Hooshmand, "An overview of control approaches of inverter-based microgrids in islanding mode of operation," *Renew. Sustain. Energy Rev.*, vol. 80, pp. 1043–1060, Dec. 2017.
[22] K. S. Ko and D. K. Sung, "The effect of EV aggregators with time-varying delays on the stability of a load frequency control system," *IEEE Trans. Power Syst.*, vol. 33, no. 1, pp. 669–680, Jan. 2018.
[23] H. Bevrani and T. Hiyama, "On load–frequency regulation with time delays: Design and real-time implementation," *IEEE Trans. Energy Convers.*, vol. 24, no. 1, pp. 292–300, Mar. 2009.
[24] H. Ameli, M. T. Ameli, and S. H. Hosseinian, "Multi-stage frequency control of a microgrid in the presence of renewable energy units," *Electr. Power Compon. Syst.*, vol. 45, no. 2, pp. 159–170, Jan. 2017.
[25] M. M. Elsaied, M. A. Attia, M. A. Mostafa, and S. F. Mekhamer, "Application of different optimization techniques to load frequency control with WECS in a multi-area system," *Electr. Power Compon. Syst.*, vol. 46, no. 7, pp. 739–756, Apr. 2018, doi: 10.1080/15325008.2018.1509913.
[26] S. Debbarma, L. C. Saikia, and N. Sinha, "AGC of a multi-area thermal system under deregulated environment using a non-integer controller," *Electr. Power Syst. Res.*, vol. 95, pp. 175–183, Feb. 2013.
[27] M. B. Delghavi, S. Shoja-Majidabad, and A. Yazdani, "Fractional-order sliding-mode control of islanded distributed energy resource systems," *IEEE Trans. Sustain. Energy*, vol. 7, no. 4, pp. 1482–1491, Oct. 2016.
[28] Y. Xie, X. Tang, S. Zheng, W. Qiao, and B. A. Song, "Adaptive fractional order PI controller design for a flexible swing arm system via enhanced virtual reference feedback tuning," *Asian J. Control*, vol. 20, no. 3, pp. 1221–1240, 2018.
[29] D. Pullaguram, S. Mishra, N. Senroy, and M. Mukherjee, "Design and tuning of robust fractional order controller for autonomous microgrid VSC system," *IEEE Trans. Ind. Appl.*, vol. 54, no. 1, pp. 91–101, Oct. 2018.
[30] S. P. Nangrani and S. S. Bhat, "Fractional order controller for controlling power system dynamic behavior," *Asian J. Control*, vol. 20, no. 1, pp. 403–414, 2018.
[31] D. Pullaguram, M. Mukherjee, S. Mishra, and N. Senroy, "Non-linear fractional order controllers for autonomous microgrid system," in *Proc. IEEE 6th Int. Conf. Power Syst. (ICPS)*, Mar. 2016, pp. 1–6.
[32] D. Maiti, S. Biswas, and A. Konar, "Design of a fractional order PID controller using particle swarm optimization technique," in *Proc. 2nd Nat. Conf. Recent Trends Inf. Syst. (ReTIS)*, 2008, pp. 1–5.
[33] T. Mahto, H. Malik, and V. Mukherjee, "Fractional order control and simulation of wind-biomass isolated hybrid power system using particle swarm optimization," in *Applications of Artificial Intelligence Techniques in Engineering*. Singapore: Springer, 2018, pp. 277–287.
[34] M.-H. Khooban, T. Niknam, M. Shasadeghi, T. Dragicevic, and F. Blaabjerg, "Load frequency control in microgrids based on a stochastic noninteger controller," *IEEE Trans. Sustain. Energy*, vol. 9, no. 2, pp. 853–861, Apr. 2018.
[35] T. S. Gorripotu, H. Samalla, J. M. Rao, A. T. Azar, and D. Pelusi, "TLBO algorithm optimized fractional-order PID controller for AGC of interconnected power system," in *Advances in Intelligent Systems and Computing*, vol. 758. Singapore: Springer, 2018, pp. 847–855.
[36] T. K. Mohapatra and B. K. Sahu, "Design and implementation of SSA based fractional order PID controller for automatic generation control of a multi-area, multi-source interconnected power system," in *Proc. Technol. Smart-City Energy Secur. Power (ICSESP)*, Mar. 2018, pp. 1–6, doi: 10.1109/icsesp.2018.8376697.
[37] M. Zamani, M. Karimi-Ghartemani, N. Sadati, and M. Parniani, "Design of a fractional order PID controller for an AVR using particle swarm optimization," *Control Eng. Pract.*, vol. 17, no. 12, pp. 1380–1387, Dec. 2009.
[38] A. T. Azar and F. E. Serrano, "Fractional order two degree of freedom PID controller for a robotic manipulator with a fuzzy type-2 compensator," in *Proc. Int. Conf. Adv. Intell. Syst. Inform.*, vol. 845, 2018, pp. 77–88.
[39] S. Mirjalili, "SCA: A sine cosine algorithm for solving optimization problems," *Knowl.-Based Syst.*, vol. 96, pp. 120–133, Mar. 2016.
[40] W. Tasnin and L. C. Saikia, "Maiden application of an sine–cosine algorithm optimised FO cascade controller in automatic generation control of multi-area thermal system incorporating dish-stirling solar and geothermal power plants," *IET Renew. Power Gener.*, vol. 12, no. 5, pp. 585–597, Apr. 2018.
[41] W. Tasnin, L. C. Saikia, and M. Raju, "Deregulated AGC of multi-area system incorporating dish-stirling solar thermal and geothermal power plants using fractional order cascade controller," *Int. J. Electr. Power Energy Syst.*, vol. 101, pp. 60–74, Oct. 2018.
[42] M. Meshkat and M. Parhizgar, "A novel sine and cosine algorithm for global optimization," in *Proc. 7th Int. Conf. Comput. Knowl. Eng. (ICCKE)*, Oct. 2017, pp. 60–65.
[43] M. Abd Elaziz, D. Oliva, and S. Xiong, "An improved opposition-based sine cosine algorithm for global optimization," *Expert Syst. Appl.*, vol. 90, pp. 484–500, Dec. 2017.
[44] M. E. Lotfy, T. Senjyu, F. M. Abdel-Fattah, A. F. Abdel-Gawad, and A. Yona, "A frequency control approach for hybrid power system using multi-objective optimization," *Energies*, vol. 10, no. 80, pp. 1–22, 2017.
[45] K. Ogata, *Modern Control Engineering*, 5th ed. Upper Saddle River, NJ, USA: Prentice-Hall, 2010.
[46] K. S. Miller and B. Ross, *An Introduction to the Fractional Calculus and Fractional Differential Equations*. New York, NY, USA: Wiley, 1993.
[47] D. Guha, P. Roy, and S. Banerjee, "Quasi-oppositional symbiotic organism search algorithm applied to load frequency control," *Swarm Evol. Comput.*, vol. 33, pp. 46–67, Apr. 2017.
[48] P. K. Roy and R. Sarkar, "Solution of unit commitment problem using quasi-oppositional teaching learning based algorithm," *Int. J. Electr. Power Energy Syst.*, vol. 60, pp. 96–106, Sep. 2014.
[49] S. M. A. Bulbul, M. Pradhan, P. K. Roy, and T. Pal, "Opposition-based krill herd algorithm applied to economic load dispatch problem," *Ain Shams Eng. J.*, vol. 9, no. 3, pp. 423–440, Sep. 2018.
[50] C. Zhang, Z. Ni, Z. Wu, and L. Gu, "A novel swarm model with quasi-oppositional particle," in *Proc. IEEE Int. Forum Inf. Technol. Appl.*, May 2009, pp. 325–330.
[51] J. Nanda, A. Mangla, and S. Suri, "Some new findings on automatic generation control of an interconnected hydrothermal system with conventional controllers," *IEEE Trans. Energy Convers.*, vol. 21, no. 1, pp. 187–194, Mar. 2006.
[52] D. Guha, P. K. Roy, and S. Banerjee, "Solutions of UPFC-based load frequency control using quasi-oppositional biogeography based optimisation considering various nonlinearities of power system," *Int. J. Power Energy Convers.*, vol. 9, no. 2, pp. 105–143, 2018.

DIPAYAN GUHA (Member, IEEE) received the Ph.D. degree in electrical engineering from the National Institute of Technology Durgapur, India, in 2017. He is currently associated with the Electrical Engineering Department, Motilal Nehru National Institute of Technology Allahabad, India. He has three years of teaching experience. He has published more than 40 research papers in International Journals and conference records. His research interests include load frequency control, distributed generation, model order reduction, intelligent control, and optimization techniques. He has been awarded with the Gold Medal in 2013. He has guided four M.Tech. students, and many are pursuing their thesis under his guidance.

PROVAS KUMAR ROY (Member, IEEE) is currently working as a Professor with the Electrical Engineering Department, Kalyani Government Engineering College, West Bengal, India. He has published a number of research papers in national/international journals and conference records. His research interests include economic load dispatch, optimal power flow, FACTS, automatic generation control, radial distribution networks, and evolutionary computing techniques.

SUBRATA BANERJEE (Senior Member, IEEE) received the Ph.D. degree in electrical engineering from IIT Kharagpur, Kharagpur, India, in 2005. He is currently a Professor with the Department of Electrical Engineering, National Institute of Technology, Durgapur, India. He has successfully completed several research and consultancy projects, including one major from DST, Government of India. He has authored/coauthored about 180 research papers in national/international journals and conference records. He has filed three Indian patents and received one Indian Patent. He has guided nine Ph.D. and 21 M.Tech. students and many are pursuing their degree under his guidance. His research interests include power electronics converters, and application of control systems in power electronics and power systems. He is a Fellow of the Institution of Engineers, India, the Institution of Electronics and Telecommunication Engineers, India, and the Institution of Engineering and Technology, U.K. He was a recipient of several academic awards, including nine Best Paper Awards and the TATA RAO Prize. His biography is included in Marquis Who's Who 2007 and IBC Foremost Engineers of the World 2008. He is acting as an Associate Editor/Editorial Board in IEEE Access, USA, and *IET Power Electronics*, U.K.

SANJEEVIKUMAR PADMANABAN (Senior Member, IEEE) received the bachelor's degree in electrical engineering from the University of Madras, Chennai, India, in 2002, the master's degree (Hons.) in electrical engineering from Pondicherry University, Puducherry, India, in 2006, and the Ph.D. degree in electrical engineering from the University of Bologna, Bologna, Italy, in 2012.

He was an Associate Professor with VIT University, from 2012 to 2013. In 2013, he joined the National Institute of Technology, India, as a Faculty Member. In 2014, he was invited as a Visiting Researcher with the Department of Electrical Engineering, Qatar University, Doha, Qatar, funded by the Qatar National Research Foundation (Government of Qatar). He continued his research activities with the Dublin Institute of Technology, Dublin, Ireland, in 2014. Further, he has served as an Associate Professor with the Department of Electrical and Electronics Engineering, University of Johannesburg, Johannesburg, South Africa, from 2016 to 2018. Since 2018, he has been a Faculty Member with the Department of Energy Technology, Aalborg University, Esbjerg, Denmark. He has authored more than 300 scientific articles.

Dr. Padmanaban is a Fellow of the Institution of Engineers, India, the Institution of Electronics and Telecommunication Engineers, India, and the Institution of Engineering and Technology, U.K. He was a recipient of the Best Paper cum Most Excellence Research Paper Awards from IET-SEISCON 2013, IET-CEAT 2016, IEEE-EECSI 2019, and IEEE-CENCON 2019; and five best paper awards from ETAEERE 2016 sponsored Lecture Notes in Electrical Engineering, Springer book. He is an Editor/Associate Editor/Editorial Board of refereed journals, in particular the IEEE Systems Journal, the IEEE Transactions on Industry Applications, IEEE Access, *IET Power Electronics*, *IET Electronics Letters*, and the *International Transactions on Electrical Energy Systems* (Wiley), a Subject Editorial Board Member of *Energy Sources* and *Energies* (MDPI) journal, and the Subject Editor of the *IET Renewable Power Generation*, *IET Generation, Transmission and Distribution*, and FACTS journal, Canada.

FREDE BLAABJERG (Fellow, IEEE) received the Ph.D. degree in electrical engineering from Aalborg University, in 1995, and the Honoris Causa degree from University Politehnica Timisoara (UPT), Romania, and Tallinn Technical University (TTU), Estonia, in 2017.

He was with ABB-Scandia, Randers, Denmark, from 1987 to 1988. He became an Assistant Professor in 1992, an Associate Professor in 1996, and a Full Professor of power electronics and drives in 1998. In 2017, he became a Villum Investigator. He has published more than 600 journal articles in the fields of power electronics and its applications. He is a coauthor of four monographs and an editor of ten books in power electronics and its applications. His current research interests include power electronics and its applications, such as in wind turbines, PV systems, reliability, harmonics, and adjustable speed drives.

Dr. Blaabjerg received 32 IEEE Prize Paper Awards, the IEEE PELS Distinguished Service Award in 2009, the EPE-PEMC Council Award in 2010, the IEEE William E. Newell Power Electronics Award in 2014, the Villum Kann Rasmussen Research Award in 2014, the Global Energy Prize in 2019, and the 2020 IEEE Edison Medal. From 2019 to 2020, he was the President of IEEE Power Electronics Society. He is the Vice-President of the Danish Academy of Technical Sciences. He is nominated in 2014–2019 by Thomson Reuters to be between the most 250 cited researchers in Engineering in the world. He was the Editor-in-Chief of the IEEE Transactions on Power Electronics, from 2006 to 2012. He has been a Distinguished Lecturer of the IEEE Power Electronics Society from 2005 to 2007 and the IEEE Industry Applications Society from 2010 to 2011 and 2017 to 2018.

DHANAMJAYULU CHITTATHURU (Member, IEEE) received the B.Tech. degree in electronics and communication engineering from JNTU University, Hyderabad, India, the M.Tech. degree in control and instrumentation systems from IIT Madras, India, and the Ph.D. degree in electronics engineering from the Vellore Institute of Technology, Vellore, India. He is currently a Faculty Member with the Control and Automation Department, School of Electrical Engineering, Vellore Institute of Technology. He is also an Assistant Professor Senior with the School of Electrical Engineering, Vellore Institute of Technology. Since 2010, he has been a Senior Assistant Professor with the Vellore Institute of Technology. His research interests include multilevel inverters, power converters, and active power filters and power quality.